

Article

Effect of ZrO₂ Content on Microstructure Evolution and Sintering Properties of (Tb_{0.7}Lu_{0.3})₂O₃ Magneto-Optic Transparent Ceramics

Yu Xin ^{1,2}, Tao Xu ¹, Yaozhi Wang ^{1,2}, Peng Luo ¹, Weiwei Li ², Bin Kang ¹, Bingchu Mei ^{2,*} and Wei Jing ^{1,*} ¹ Institute of Chemical Materials, China Academy of Engineering Physics, Mianyang 621900, China² State Key Laboratory of Advanced Technology for Materials Synthesis and Processing, Wuhan University of Technology, Wuhan 430070, China

* Correspondence: bcmei@whut.edu.cn (B.M.); jingwei@caep.cn (W.J.)

Abstract: In this paper, (Tb_{0.7}Lu_{0.3})₂O₃ magneto-optical transparent ceramics with different ZrO₂ doping levels (0~5 at%) were prepared by hydrogen sintering and sequential HIP technique using ZrO₂ as a sintering aid. The effect of ZrO₂ doping content on the microstructure and optical properties of (Tb_{0.7}Lu_{0.3})₂O₃ ceramics was analyzed. We found that the optimal doping content of ZrO₂ was 3 at%. The transmittance of 3 at% ZrO₂-doped (Tb_{0.7}Lu_{0.3})₂O₃ ceramics at the wavelength of 1064 nm was 74.84 %, and the Verdet constant was approximately 275.28 rad·T⁻¹·m⁻¹ at the wavelength of 650 nm.

Keywords: magneto-optic ceramics; Tb₂O₃; Lu₂O₃; ZrO₂; microstructure; sintering properties



Citation: Xin, Y.; Xu, T.; Wang, Y.; Luo, P.; Li, W.; Kang, B.; Mei, B.; Jing, W. Effect of ZrO₂ Content on Microstructure Evolution and Sintering Properties of (Tb_{0.7}Lu_{0.3})₂O₃ Magneto-Optic Transparent Ceramics. *Magnetochemistry* **2022**, *8*, 175. <https://doi.org/10.3390/magnetochemistry8120175>

Academic Editor: Jiang Li

Received: 30 October 2022

Accepted: 28 November 2022

Published: 1 December 2022

Publisher's Note: MDPI stays neutral with regard to jurisdictional claims in published maps and institutional affiliations.



Copyright: © 2022 by the authors. Licensee MDPI, Basel, Switzerland. This article is an open access article distributed under the terms and conditions of the Creative Commons Attribution (CC BY) license (<https://creativecommons.org/licenses/by/4.0/>).

1. Introduction

A magneto-optical element (MOE) is one of the crucial components of Faraday rotators and isolators and can eliminate reflected light to ensure the stability of laser transmission in the laser system [1–4]. Usually, magneto-optical materials with high Verdet constants are chosen for MOEs because small magneto-optical materials are required if the Verdet constant is high according to the Faraday effect formula of $\theta = VBL$, where V is the Verdet constant, θ is the rotation angle of the light vector and L is the length of the magneto-optical material.

At present, a TGG (Terbium gallium garnet) single crystal with a Verdet constant of approximately $-134 \text{ rad}\cdot\text{T}^{-1}\cdot\text{m}^{-1}$ is the most widely used magneto-optical material [5–7]. However, owing to the size limitation of the crystal material and the relatively low Verdet constant, sesquioxide materials with higher Verdet constants, such as holmium oxide, terbium oxide, etc. [8–10], have attracted considerable attention. Among the sesquioxides, Tb₂O₃ has many excellent properties, such as high angular momentum [11] and only one absorption peak at 483 nm [12]. However, terbium sesquioxide easily oxidizes into Tb₄O₇ without magneto-optical properties, which considerably affect the performance of this kind of material [13]. Furthermore, terbium oxide undergoes a reversible phase transition from the C-type cubic phase to the B-type monoclinic phase when the temperature exceeds 1600 °C. [14,15].

In order to prevent oxidation of terbium oxide, commercial Tb₂O₃ powders were used as original powder and sintered in an oxygen-free environment [16]. Some researchers attempted to deoxidize commercial Tb₄O₇ powder to Tb₂O₃ powder by hydrogen sintering [17] to reduce the sintering temperature. In the view of the phase change of terbium oxide during sintering, researchers have proposed a solution of doping rare earth elements [18–20]. Moreover, sintering additives including ZrO₂, La₂O₃, MgO, etc., were added to reduce the sintering temperature [21,22]. All these strategies represent promising techniques.

In 2017, Ning et al. [23] used low-level (0.5 wt%) ZrO₂-MgO as a double-sintering aid to prepare highly transparent Yb:Y₂O₃ ceramics. The addition of 0.5 wt% ZrO₂ was found to effectively increase the density of the ceramics and promote pore elimination. In 2019, Hu et al. [24] prepared Dy₂O₃ transparent ceramics by vacuum sintering of nanopowders. A Dy₂O₃ phase appeared at 600 °C during the decomposition period of the precursor, and the in-line transmittance values of the optimal ceramic sample with 1.0 mm thickness are 75.3% at 2000 nm and 67.9% at 633 nm. Despite many studies on Yb₂O₃, Dy₂O₃ and other sesquioxide materials, few studies have investigated the effect of sintering additives on the sintering properties of Tb₂O₃ ceramics.

In this work, (Tb_{0.7}Lu_{0.3})₂O₃ transparent ceramics were prepared by hydrogen pre-sintering combined with hot isostatic pressing sintering. We added varying amounts of ZrO₂ as sintering aids to promote ceramic densification. The effect of ZrO₂ content on the microstructure and sintering properties of these samples were investigated.

2. Experiment

2.1. Preparation Processes

High-purity Tb₂O₃ (99.99%), Lu₂O₃ (99.99%) and ZrO₂ (99.99%) powders were used as raw materials. The raw materials were weighted according to the chemical formula of (Tb_{0.7}Lu_{0.3})₂O₃ and 0~5 at% ZrO₂ and mixed by ball milling for 24 h at a speed of 200 r/min. After drying by rotary evaporator, the dried powders were sieved through 100 meshes. The green ceramic samples were dry-pressed into a disk with a diameter of 20 mm at 20 MPa and further cold isostatically pressed at 200 MPa for 120s to increase the density. Before hydrogen sintering, the samples were calcined at 1000 °C for 10 h to remove organic impurities and residual carbon. The green bodies were sintered between 1550 °C and 1700 °C for 4 h in a hydrogen atmosphere. All the presintered samples were hot isostatically pressed at 1575 °C in an argon atmosphere to eliminate closed pores to improving performance of the ceramics. Finally, transparent (Tb_{0.7}Lu_{0.3})₂O₃ ceramics were obtained by mirror polishing to 2.0 mm thickness for measurement.

2.2. Characterization

The phase compositions of the ceramics were determined by X-ray diffraction (XRD; DX-1000CSC, Tongda Co. Ltd., Dandong, Liaoning, China) using Cu K α radiation with a scan speed of 10°/min and a step size of 0.03° in the range of 2 θ = 10°–70°. The linear shrinkage rate of the ceramics was calculated according to the following formula:

$$\frac{\Delta L}{L_0} = \frac{L_1 - L_0}{L_0} \quad (1)$$

where ΔL is the linear shrinkage of the sample after sintering, L_0 is the size of the green body before sintering and L_1 is the size of the samples after sintering. Microstructures of the fracture surfaces were examined using field emission scanning electron microscopy (SEM, Inspect F, FEI, Hillsborocity, OR, USA). The in-line transmittance of ceramics was measured by a UV-VIS-NIR spectrometer (Lambda950, PerkinElmer, Waltham, MA, USA) over the wavelength region from 200 nm to 1600 nm. Verdet constants were recorded on a Faraday effect experimental instrument (FD-FZ-C, Shanghai Fudan Tianxin Scientific & Educational Instruments Co., Ltd., Shanghai, China), with a laser wavelength of 650 nm.

3. Result and Discussion

Figure 1 presents XRD patterns of the (Tb_{0.7}Lu_{0.3})₂O₃ ceramic samples with varying Zr⁴⁺ concentrations after hot isostatic pressing sintering. Compared with the standard XRD spectra of Lu₂O₃ (PDF#74-1980) and Tb₂O₃ (PDF#43-1012), there is no other impurity phase, and all the samples are approximately consistent with the characteristic peak of Tb₂O₃. The four diffraction peaks at 29°, 33.6°, 48.5° and 57.64° in the figure correspond to the crystal face of the cubic phases Tb₂O₃ (222), (400), (440) and (622), respectively [11]. The diffraction patterns located between the diffraction patterns of Tb₂O₃ and Lu₂O₃ indicate

that the Lu^{3+} successfully entered the Tb_2O_3 lattice and replaced the Tb^{3+} sites to form a $(\text{Tb}_{0.7}\text{Lu}_{0.3})_2\text{O}_3$ solid solution.

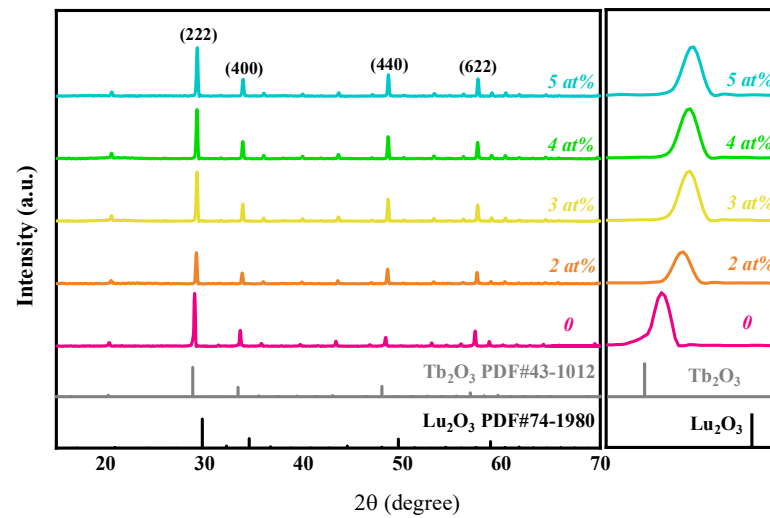
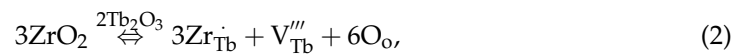


Figure 1. XRD patterns of $(\text{Tb}_{0.7}\text{Lu}_{0.3})_2\text{O}_3$ ceramics with 0–5 at% ZrO_2 as sintering aids after hot isostatic pressing sintering.

With the increase in ZrO_2 content, the characteristic peak shifts towards higher angles, which can be explained by the formulae (2) and (3), for which the standard notations of Kröger and Vink were used [25]. According to previous research [23], when ZrO_2 is added as a sintering aid, Zr^{4+} replaces the position of $\text{Tb}^{3+}/\text{Lu}^{3+}$, and the following reactions occur to generate cation vacancies, which reduce the cell volume.



In addition, the radius of Zr^{4+} (0.072 nm) is smaller than that of Tb^{3+} (0.0923 nm) and Lu^{3+} (0.0861 nm), which may also decrease the lattice cell constant.

Figure 2 shows the changes in lattice constant calculated by the XRD patterns. The cell size of the undoped $(\text{Tb}_{0.7}\text{Lu}_{0.3})_2\text{O}_3$ ceramic is approximately 10.4 angstrom. When zirconia is added from 2 at% to 3 at%, the cell size decreases from 10.37 Å to 10.35 Å. However, the lattice constant does not change linearly with the zirconia content. When the zirconia content exceeds 4 at%, the change in lattice constant is not obviously (approximately 0.01 Å), which could be ascribed to the zirconia solid solubility limit. The excess zirconia cannot enter the lattice, with an insignificant effect on the lattice constant. When the zirconia content is 5 at%, the lattice constant is 10.35 Å.

Figure 3 shows the change in linear shrinkage of $(\text{Tb}_{0.7}\text{Lu}_{0.3})_2\text{O}_3$ ceramics with varying ZrO_2 contents after hydrogen sintering from 1550 °C to 1700 °C. As shown in the figure, linear shrinkage increases with increased temperature. The shrinkage of the samples increases with increased zirconia content at the same sintering temperature. The linear shrinkage rate of the sample with no additional sintering additives increased linearly in the range of 1550 °C to 1700 °C. However, when ZrO_2 was added, a plateau gradually appeared around the temperature of 1600 °C–1650 °C, and the curve of those samples with zirconia as a sintering aid could be divided into two sections. Before 1600 °C, the sample shrank rapidly, and the curve slope was relatively high. When the temperature exceeded 1600 °C, the slope was reduced with increased Zr^{4+} doping, proving that ZrO_2 can improve the densification rate and that ceramics can be rapidly densified below 1600 °C with sufficient zirconia content. The shrinkage curves were nearly identical when the doping content of Zr^{4+} exceeded 3 at%.

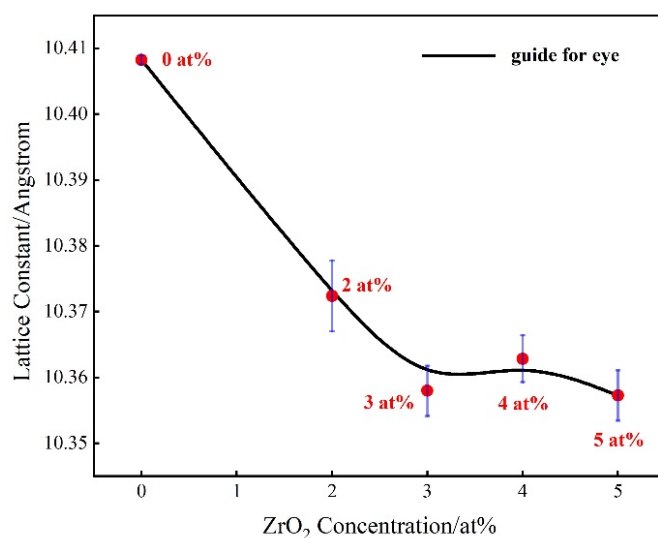


Figure 2. Change in lattice constants with varying Zr concentrations.

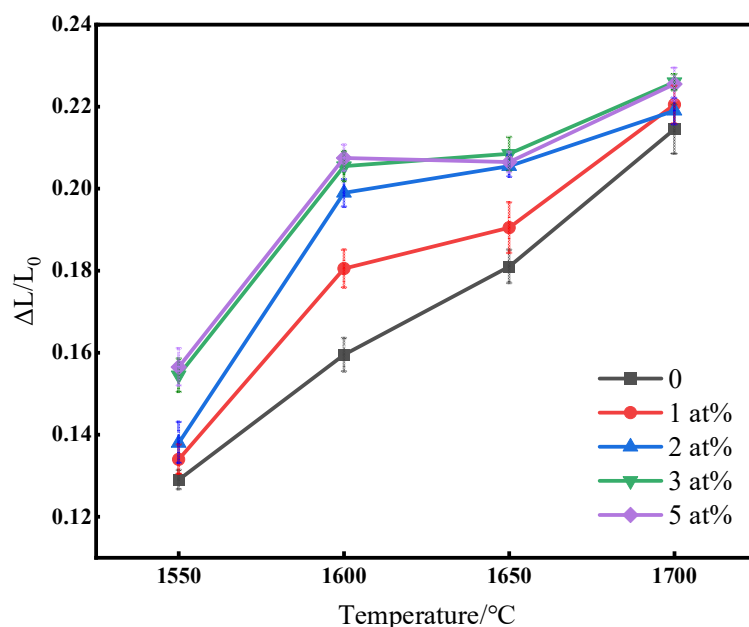


Figure 3. Linear shrinkage rate with varying ZrO₂ contents after hydrogen sintering from 1550 °C to 1700 °C.

According to the results presented above, we presintered the ceramics in a hydrogen atmosphere at 1550 °C, combined with hot isostatic pressing sintering at 1575 °C to make the samples fully dense. Tb₂O₃ undergoes severe phase transformation at 1600 °C [12,13], so a relatively low sintering temperature was chosen to avoid this transformation.

The microstructure of (Tb_{0.7}Lu_{0.3})₂O₃ ceramics after hydrogen sintering at 1550 °C with varying ZrO₂ contents is shown in Figure 4. With an increase in Zr⁴⁺ content from 0 to 3 at%, the pores become smaller, suggesting that the addition of ZrO₂ can effectively reduce the sintering barrier of (Tb_{0.7}Lu_{0.3})₂O₃ ceramics and promote pore elimination during presintering. Subsequently, the phenomenon of pore shrinkage became indistinct when the addition amount increased to 4 at%. As shown in Figure 4e, the porosity and pore size increased considerably, suggesting that excessive zirconia is unfavorable for pore elimination during the presintering process.

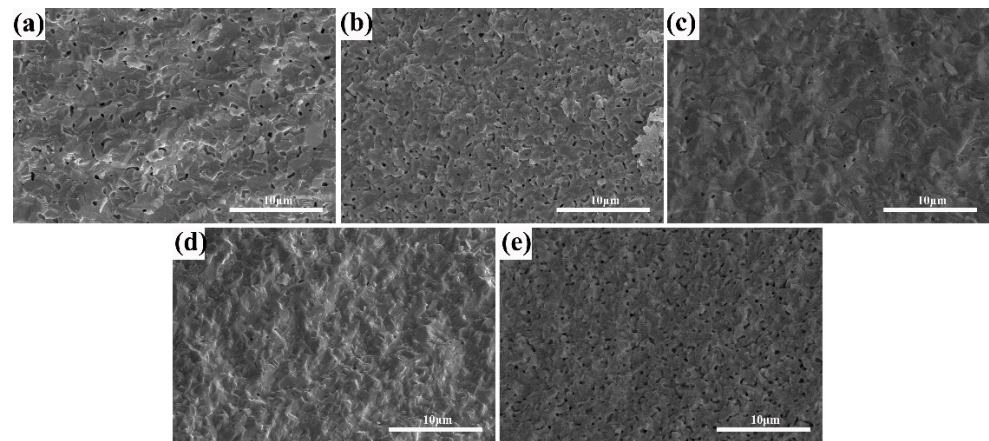


Figure 4. SEM photomicrographs of the fractured surfaces of the $(\text{Tb}_{0.7}\text{Lu}_{0.3})_2\text{O}_3$ ceramics after 1500 °C hydrogen sintering with varying ZrO_2 contents: (a) 0 at%, (b) 2 at%, (c) 3 at%, (d) 4 at%, (e) 5 at%.

Figure 5 shows SEM image of the ceramics with varying ZrO_2 contents after hot isostatic pressing sintering. The samples showed mainly transcrystalline fractures, and all samples presented with high density. As shown in Figure 5a, a large number of intragranular pores were observed, with a relatively large grain size.

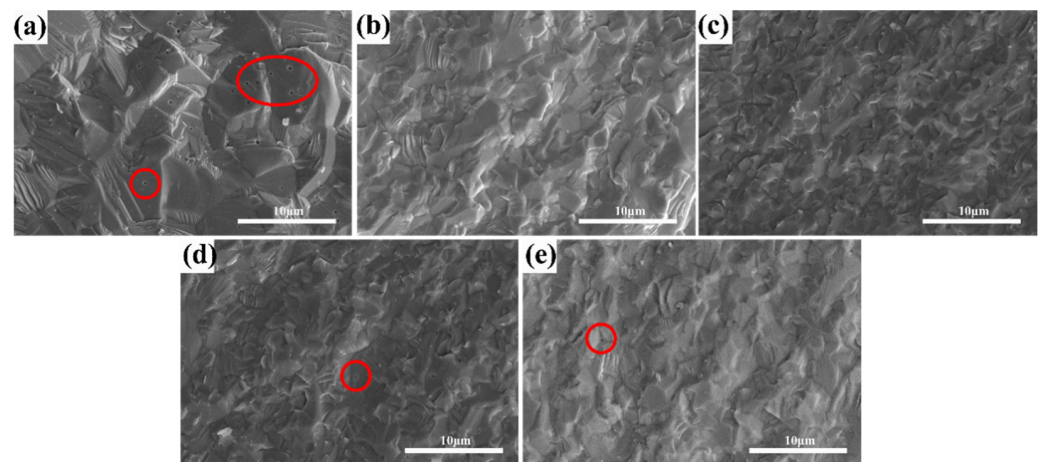


Figure 5. SEM micrographs of the fractured surfaces of the $(\text{Tb}_{0.7}\text{Lu}_{0.3})_2\text{O}_3$ ceramics after 1575 °C hot isostatic pressing sintering with varying ZrO_2 contents (The pores were marked in red circles): (a) 0 at%, (b) 2 at%, (c) 3 at%, (d) 4 at%, (e) 5 at%.

On the contrary, no obvious pores can be observed in Figure 5b,c. When Zr content exceeds 3 at%, some intragranular pores can be observed in Figure 5d,e. The grain size decreases from 2.23 μm to 1.92 μm with increased ZrO_2 content, which could be attributed to the doping effect of ZrO_2 , which has been reported in many other sesquioxide ceramic sintering processes [26–29]. During the high-temperature sintering process of sesquioxide ceramics, the sintering aid, ZrO_2 , can enter the lattice of sesquioxide as Zr^{4+} , as shown in Formulae (2) and (3). It can inhibit the rapid growth of ceramic grains, avoid the formation of intracrystalline pores and contribute to the full densification of ceramics. As shown in the figure, this effect is closely related to the concentration of zirconia. When the concentration is 3 at% or less, the densification of zirconia is considerable, but a further increase in the content can result in densifying hazards.

Figure 6 shows the in-line transmittance and appearance of $(\text{Tb}_{0.7}\text{Lu}_{0.3})_2\text{O}_3$ transparent ceramics with varying contents of ZrO_2 additive. Figure 6a shows that the samples sintered with ZrO_2 exhibited sufficient optical quality, so the words below the ceramics

could be clearly seen, and the optical quality was better than that of the ceramic sample without additive. This result is also confirmed by the transmittance curve of the sample shown in Figure 6b. The sample without sintering additives has the lowest transmittance, which could be related to the intracrystalline pores, as shown in Figure 5. With increased Zr^{4+} content, the transparency first increased and then decreased, which is also related to the effect of zirconia. When zirconia content is excessive, it changes the sintering properties of the material, simultaneously affecting the internal microstructure (as shown in Figures 4 and 5), ultimately reducing the transparency. The ceramic sample with 3 at% ZrO_2 addition has the best optical quality, with a transparency of 74.96% at 1064 nm and 75.01% at 1550 nm. However, the transparency decreases with a further increase in Zr^{4+} content to 4 at%, which could be related to the change in the internal microstructure of the ceramics. All the transmission curves show obvious emission peaks at 483 nm, in association with the Tb^{3+} energy transition from 7F_6 to 5D_4 [11].

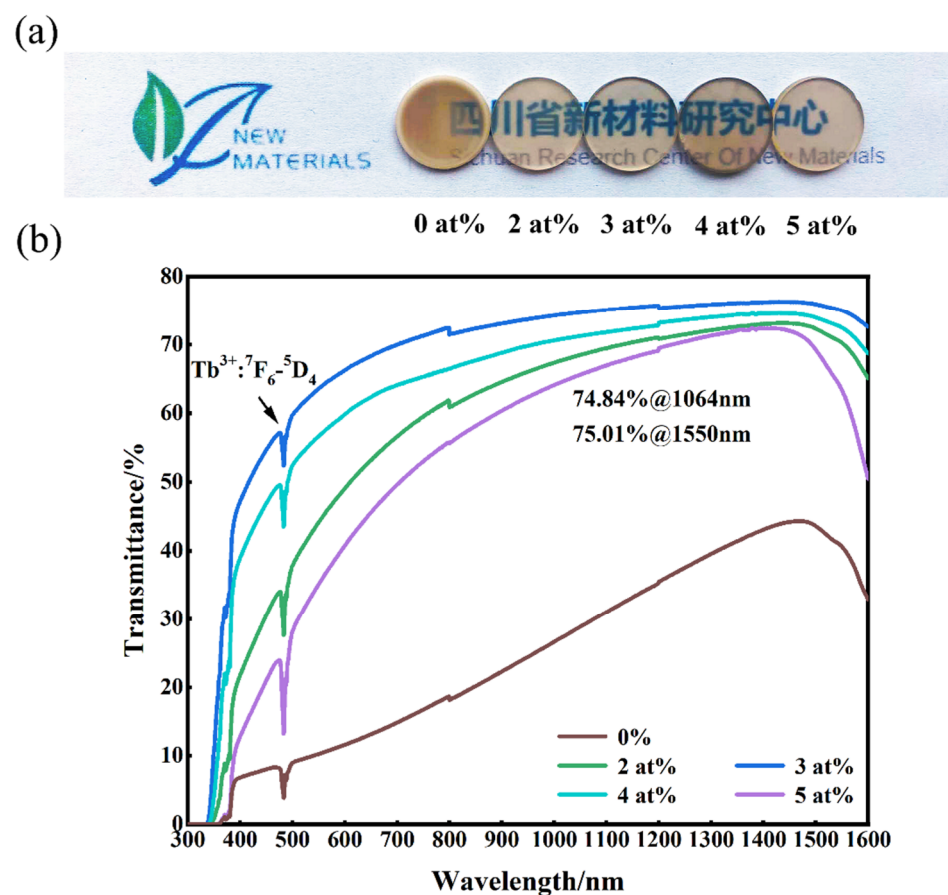


Figure 6. Photograph (a), and in-line transmittances curves (b) of the mirror-polished $(Tb_{0.7}Lu_{0.3})_2O_3$ ceramics sintered at 1550 °C followed by HIP at 1575 °C. (Zirconia content from left to right is 0 at%, 2 at%, 3 at%, 4 at% and 5 at%).

Figure 7a shows the microstructure of 3 at% ZrO_2 doped $(Tb_{0.7}Lu_{0.3})_2O_3$ ceramics. The fracture surface exhibited a pore-free structure, and the grains were tightly bound to each other. In addition, no secondary phase grain was observed on the grain boundary. As shown in Figure 5b, the particle size distribution of 3 at% Zr: $(Tb_{0.7}Lu_{0.3})_2O_3$ is mainly in the range of 1.0–2 μm , and the average grain size is approximately 1.74 μm .

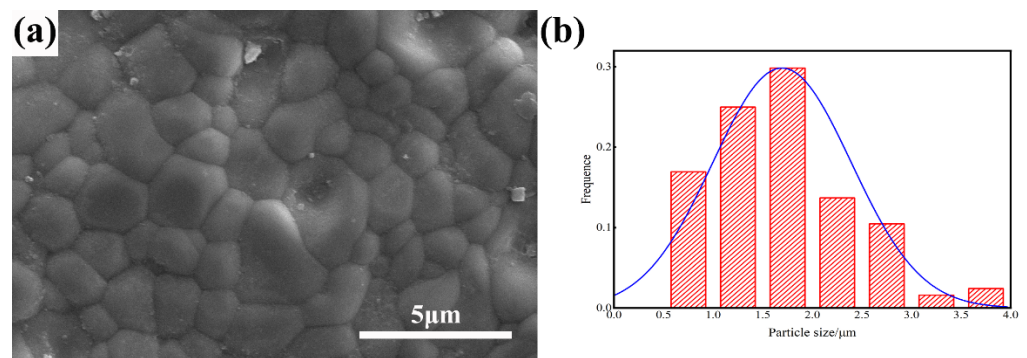


Figure 7. SEM micrographs of the surface of 3 at% Zr: $(\text{Tb}_{0.7}\text{Lu}_{0.3})_2\text{O}_3$ ceramic after hot isostatic pressing sintering (a) and the particle size distribution (b).

Figure 8 shows the Verdet constant of $(\text{Tb}_{0.7}\text{Lu}_{0.3})_2\text{O}_3$ ceramics with varying Zr^{4+} contents at the 650 nm wavelength at room temperature. The Verdet constants for the ceramic samples were calculated using the following formula:

$$\theta = VHL \quad (4)$$

where V is the Verdet constant, θ is the rotation angle of the light vector and L is the length of the magneto-optical material. All samples were polished to 2 mm. As shown in the figure, the Verdet constant decreases from $339.36 \text{ rad}\cdot\text{T}^{-1}\cdot\text{m}^{-1}$ to $235.22 \text{ rad}\cdot\text{T}^{-1}\cdot\text{m}^{-1}$ with an increase in Zr^{4+} content from 0 at% to 5 at%. The Verdet constants of $(\text{Tb}_{0.7}\text{Lu}_{0.3})_2\text{O}_3$ ceramics changed depending on the Zr^{4+} concentration. According to the literature [30,31], for Tb^{3+} ions, there are unpaired free electrons on the 4f electron layer, which produce an uncompensated magnetic moment in the magnetic field, which is the source of the magnetism. In the external magnetic field, electrons are prone to $^4f_8-^4f_7^5d$ transitions, which correspond to $^7F_6-^7D_5$ level transition, demonstrating strong magnetism.

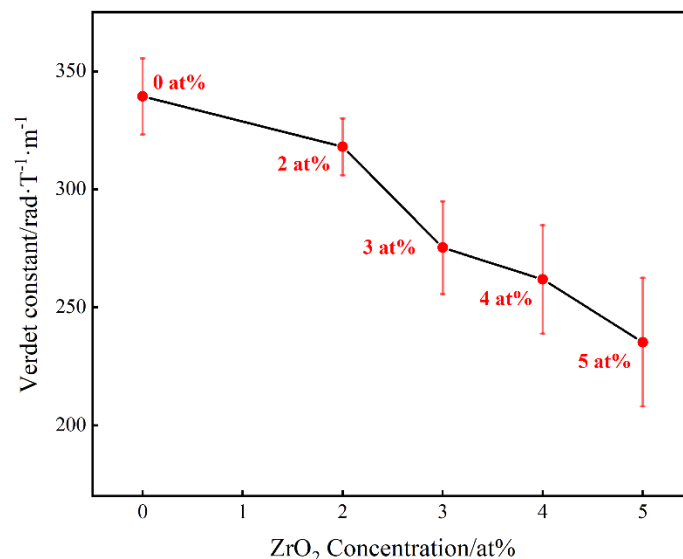


Figure 8. Verdet constant of Zr: $(\text{Tb}_{0.7}\text{Lu}_{0.3})_2\text{O}_3$ ceramics versus Zr^{4+} concentration at the 650 nm wavelength at room temperature.

This phenomenon can be explained as follows. A large number of lattice vacancies and defects are produced with the addition of ZrO_2 , which may affect the electron transition of Tb^{3+} , with an eventual decrease in the Verdet constant. Although the Verdet constant decreases with increased Zr^{4+} content, the Verdet constant of $(\text{Tb}_{0.7}\text{Lu}_{0.3})_2\text{O}_3$ ceramics with

3 at% ZrO₂ is 275.28 rad·T⁻¹·m⁻¹, which is still about 2.05 times that of a commercial TGG single crystal.

4. Conclusions

Highly transparent (Tb_{0.7}Lu_{0.3})₂O₃ ceramics were prepared using ZrO₂ as a sintering additive via hot isostatic pressing sintering process. With increased Zr⁴⁺ content, the grain size decreases; the transparency of the sample increases first and then decreases. The inline transmittance of 3 at% ZrO₂ doped (Tb_{0.7}Lu_{0.3})₂O₃ ceramics reached 74.84% at 1064 nm. The addition of ZrO₂ can effectively reduce the sintering barrier of (Tb_{0.7}Lu_{0.3})₂O₃ ceramics, inhibit the abnormal growth of grains and promote the discharge of pores. The average grain size of the ceramics with 3 at% ZrO₂ added is approximately 1.74 μm. The Verdet constant of 3 at% ZrO₂-doped ceramics is 275.28 rad·T⁻¹·m⁻¹, which is still approximately 2.05 times that of a commercial TGG single crystal.

Author Contributions: Conceptualization, W.J.; Methodology, Y.X., T.X. and W.J.; Data analysis, Y.X., Y.W. and P.L.; Resources, B.K., W.J. and B.M.; Supervision, B.K. and W.J.; Writing—original draft, Y.X.; Writing—review and editing, W.J. and W.L. All authors have read and agreed to the published version of the manuscript.

Funding: This work was supported by the Development Foundation of China Academy of Engineering Physics and the National Natural Science Foundation of China (Grant No. 51902234).

Institutional Review Board Statement: Not applicable.

Informed Consent Statement: Not applicable.

Data Availability Statement: The data presented in this study are available upon request from the corresponding authors.

Conflicts of Interest: The authors declare no conflict of interest.

References

1. Bayramian, A.; Armstrong, J.; Beer, G.; Campbell, R.; Chai, B.; Cross, R.; Erlandson, A.; Fei, Y.; Freitas, B.; Kent, R.; et al. High-average-power femto-petawatt laser pumped by the Mercury laser facility. *J. Opt. Soc. Am. B* **2008**, *25*, B57–B61. [[CrossRef](#)]
2. Mueller, G.; Amin, R.S.; Guagliardo, D.; McFeron, D.; Lundock, R.; Reitze, D.H.; Tanner, D. Method for compensation of thermally induced modal distortions in the input optical components of gravitational wave interferometers. *Class. Quantum Gravity* **2002**, *19*, 1793–1801. [[CrossRef](#)]
3. Khazanov, E.; Andreev, N.; Mal'Shakov, A.; Palashov, O.; Poteomkin, A.; Sergeev, A.; Shaykin, A.; Zelenogorsky, V.; Ivanov, I.; Amin, R.; et al. Compensation of thermally induced modal distortions in Faraday isolators. *IEEE J. Quantum Electron.* **2004**, *40*, 1500–1510. [[CrossRef](#)]
4. Dai, J.; Li, J. Promising magneto-optical ceramics for high power Faraday isolators. *Scr. Mater.* **2018**, *155*, 78–84. [[CrossRef](#)]
5. Yasuhara, R.; Nozawa, H.; Yanagitani, T.; Motokoshi, S.; Kawanaka, J. Temperature dependence of thermo-optic effects of single-crystal and ceramic TGG. *Opt. Express* **2013**, *21*, 31443–31452. [[CrossRef](#)]
6. Chen, Z.; Hang, Y.; Wang, X.; Hong, J. Fabrication and characterization of TGG crystals containing paramagnetic rare-earth ions. *Solid State Commun.* **2016**, *241*, 38–42. [[CrossRef](#)]
7. Wu, Y.; Sun, Z.; Feng, G.; Wang, S.; Xu, L.; Wu, S. Preparation and properties of novel Tb₃Sc₂Al₃O₁₂ (TSAG) magneto-optical transparent ceramic. *J. Eur. Ceram. Soc.* **2021**, *41*, 195–201. [[CrossRef](#)]
8. Furuse, H.; Yasuhara, R. Magneto-optical characteristics of holmium oxide (Ho₂O₃) ceramics. *Opt. Mater. Express* **2017**, *7*, 827–833. [[CrossRef](#)]
9. Yakovlev, A.; Snetkov, I.; Permin, D.; Balabanov, S.; Palashov, O. Faraday rotation in cryogenically cooled dysprosium based (Dy₂O₃) ceramics. *Scr. Mater.* **2018**, *161*, 32–35. [[CrossRef](#)]
10. Veber, P.; Velázquez, M.; Gadret, G.; Rytz, D.; Peltz, M.; Decourt, R. Flux growth at 1230 °C of cubic Tb₂O₃ single crystals and characterization of their optical and magnetic properties. *CrystEngComm* **2014**, *17*, 492–497. [[CrossRef](#)]
11. Ibáñez, J.; Sans, J.Á.; Cuenca-Gotor, V.; Oliva, R.; Gomis, Ó.; Rodríguez-Hernández, P.; Muñoz, A.; Rodríguez-Mendoza, U.; Velázquez, M.; Veber, P.; et al. Structural and Lattice-Dynamical Properties of Tb₂O₃ under Compression: A Comparative Study with Rare Earth and Related Sesquioxides. *Inorg. Chem.* **2020**, *59*, 9648–9666. [[CrossRef](#)] [[PubMed](#)]
12. Snetkov, I.; Yakovlev, A.; Starobor, A.; Balabanov, S.; Permin, D.; Rostokina, E.; Palashov, O. Thermo-optical properties of terbium sesquioxide (Tb₂O₃) ceramics at room temperature. *Opt. Lett.* **2021**, *46*, 3592–3595. [[CrossRef](#)] [[PubMed](#)]

13. Wang, Y.; Jing, W.; Li, W.; Xu, T.; Kang, B.; Liu, X.; Xin, Y.; Luo, P.; Yang, N.; Mei, B. Synthesis of highly sinterable Tb₂O₃ powders by spray coprecipitation for transparent ceramics: The influence of ammonium hydrogen carbonate to metal ions molar ratio. *Opt. Mater.* **2022**, *132*, 112795. [[CrossRef](#)]
14. Zhang, J.; Chen, H.; Wang, J.; Wang, D.; Han, D.; Zhang, J.; Wang, S. Phase transformation process of Tb₂O₃ at elevated temperature. *Scr. Mater.* **2019**, *171*, 108–111. [[CrossRef](#)]
15. Lee, C.; Vashishtha, S.; Sayal, A.; Weaver, J.F. Oxidation of a c-Tb₂O₃ (111) thin film by the sequential formation of stoichiometric phases. *Surf. Sci.* **2019**, *694*, 121555. [[CrossRef](#)]
16. Zhang, J.; Chen, H.; Wang, J.; Wang, D.; Han, D.; Zhang, J.; Wang, S. Preparation of (Tb_{1-x}Lu_x)₂O₃ transparent ceramics by solid solution for magneto-optical application. *J. Eur. Ceram. Soc.* **2021**, *41*, 2818–2825. [[CrossRef](#)]
17. Yang, M.; Zhou, D.; Xu, J.; Tian, T.; Jia, R.; Wang, Z. Fabrication and magneto-optical property of yttria stabilized Tb₂O₃ transparent ceramics. *J. Eur. Ceram. Soc.* **2019**, *39*, 5005–5009. [[CrossRef](#)]
18. Zhu, L.; Park, Y.; Gan, L.; Go, S.; Kim, H.; Kim, J.; Ko, J. Fabrication and characterization of highly transparent Er: Y₂O₃ ceramics with ZrO₂ and La₂O₃ additives. *Ceram. Int.* **2017**, *43*, 13127–13132. [[CrossRef](#)]
19. Yi, Q.; Zhou, S.; Teng, H.; Lin, H.; Hou, X.; Jia, T. Structural and optical properties of Tm: Y₂O₃ transparent ceramic with La₂O₃, ZrO₂ as composite sintering aid. *J. Eur. Ceram. Soc.* **2012**, *32*, 381–388. [[CrossRef](#)]
20. Xie, J.; Mao, X.; Zhu, Q.; Jiang, B.; Zhang, L. Influence of synthesis conditions on the properties of Y₂O₃-MgO nanopowders and sintered nanocomposites. *J. Eur. Ceram. Soc.* **2017**, *37*, 4095–4101. [[CrossRef](#)]
21. Snetkov, I.L.; Permin, D.A.; Balabanov, S.S.; Palashov, O.V. Wavelength dependence of Verdet constant of Tb³⁺: Y₂O₃ ceramics. *Appl. Phys. Lett.* **2016**, *108*, 161905. [[CrossRef](#)]
22. Ikesue, A.; Aung, Y.L.; Makikawa, S.; Yahagi, A. Polycrystalline (Tb_xY_{1-x})₂O₃ Faraday rotator. *Opt. Lett.* **2017**, *42*, 4399–4401. [[CrossRef](#)] [[PubMed](#)]
23. Ning, K.; Wang, J.; Luo, D.; Dong, Z.L.; Kong, L.B.; Tang, D.Y. Low-level sintering aids for highly transparent Yb: Y₂O₃ ceramics. *J. Alloy. Compd.* **2017**, *695*, 1414–1419. [[CrossRef](#)]
24. Hu, D.; Liu, X.; Liu, Z.; Li, X.; Tian, F.; Zhu, D.; Yang, Z.; Wu, L.; Li, J. Fabrication of Dy₂O₃ Transparent Ceramics by Vacuum Sintering Using Precipitated Powders. *Magnetochemistry* **2021**, *7*, 6. [[CrossRef](#)]
25. Kröger, F.A.; Vink, H.J. Relations between the concentrations of imperfections in solids. *J. Phys. Chem. Solids* **1958**, *5*, 208–223. [[CrossRef](#)]
26. Bokuniaeva, A.O.; Vorokh, A.S. Estimation of particle size using the Debye equation and the Scherrer formula for polyphasic TiO₂ powder. *J. Phys. Conf. Ser.* **2019**, *1410*, 012057. [[CrossRef](#)]
27. Hou, X.; Zhou, S.; Li, Y.; Li, W. Effect of ZrO₂ on the sinterability and spectral properties of (Yb_{0.05}Y_{0.95})₂O₃ transparent ceramic. *Opt. Mater.* **2010**, *32*, 920–923. [[CrossRef](#)]
28. Jin, L.; Zhou, G.; Shimai, S.; Zhang, J.; Wang, S. ZrO₂-doped Y₂O₃ transparent ceramics via slip casting and vacuum sintering. *J. Eur. Ceram. Soc.* **2010**, *30*, 2139–2143. [[CrossRef](#)]
29. Li, X.; Xu, Y.; Mao, X.; Zhu, Q.; Xie, J.; Feng, M.; Jiang, B.; Zhang, L. Investigation of optical, mechanical, and thermal properties of ZrO₂-doped Y₂O₃ transparent ceramics fabricated by HIP. *Ceram. Int.* **2018**, *44*, 1362–1369. [[CrossRef](#)]
30. Yang, H.; Zhu, Z. Magneto-optical glass mixed with Tb³⁺ ions: High Verdet constant and luminescence properties. *J. Lumin.* **2021**, *231*, 117804. [[CrossRef](#)]
31. Yin, H.; Gao, Y.; Gong, Y.; Buchanan, R.; Song, J.; Li, M. Wavelength dependence of Tb³⁺ doped magneto-optical glass Verdet constant. *Ceram. Int.* **2018**, *44*, 10929–10933. [[CrossRef](#)]